

Enhanced Quantum Sensing with Hybrid Exceptional-Diabolic Singularities

Javid Naikoo,^{1,*} Ravindra W. Chhajlany,¹ and Adam Miranowicz¹

¹*Institute of Spintronics and Quantum Information, Faculty of Physics and Astronomy, Adam Mickiewicz University, 61-614 Poznań, Poland*
(Dated: February 7, 2025)

We report an enhanced sensitivity for detecting linear perturbations near hybrid (doubly degenerated) exceptional-diabolic (HED) singular points in a four mode bosonic system. The sensitivity enhancement is attributed to a singular response function, with the pole order determining the scaling of estimation error. At HED singular points, the error scaling exhibits a twofold improvement over non-HED singular points. The ultimate bound on estimation error is derived via quantum Fisher information, with heterodyne detection identified as the measurement achieving this optimal scaling.

I. INTRODUCTION

The study of non-Hermitian systems, which feature complex eigenvalues, has gained significant attention due to their intriguing and unconventional properties. A key phenomenon in such systems is the presence of *exceptional points* (EPs)—*singularities* in the complex energy plane where both eigenvalues and eigenvectors coalesce. First studied in physical context in [1], EPs arise in parameter-dependent eigenvalue problems and are encountered in a wide range of physical systems, such as optics, mechanics, quantum phase transitions, and quantum chaos [2–5]. In contrast, *diabolic points* (DPs), introduced in [6], arise in Hermitian systems as instances of eigenvalue degeneracies where eigenvectors remain orthogonal. These points are closely associated with geometric phases and Berry’s curvature. Remarkably, certain non-Hermitian systems can exhibit both EPs and DPs, with their intersections giving rise to *hybrid exceptional-diabolic* (HED) points. These HED points blend the distinct features of both singularities and offers valuable insights into the interplay between Hermitian and non-Hermitian physics unlocking potential applications across diverse physical domains [7–10].

Recent advances in quantum sensing have highlighted the transformative potential of non-Hermitian systems in achieving ultra-sensitive measurements, especially through the use of exceptional point singularities, where small perturbations lead to disproportionately large responses. This property can dramatically amplify sensitivity, offering a pathway to high-precision measurements that would be infeasible in Hermitian frameworks [11–14]. A system near an EP, when perturbed, displays eigenvalue splitting that scales as the n th root of the perturbation size ($\sim \sqrt[n]{\epsilon}$), yielding a steep sensitivity that can surpass what is achievable in Hermitian settings where perturbations result in linear or quadratic responses [15]. Experimental work with optical resonators has validated this principle, demonstrating that under carefully controlled conditions, non-Hermitian systems can achieve extremely sensitive measurements [16, 17]. However, under real-world noise conditions, this sensitivity is typically limited by quantum noise, which can diminish the response and limit the achievable gains [18–26].

In particular, [18, 23] argue convincingly that EP sensors do not provide any fundamental improvement in signal-to-noise ratio (SNR), challenging the notion that exceptional points inherently enhance sensor performance. Building on this, [19] highlights that enhanced sensitivity is primarily driven by nonreciprocity rather than the proximity to an exceptional point. This study establishes fundamental bounds on signal power and SNR for two-mode sensors, demonstrating that while gain is necessary for enhanced signal power, it does not rely on being near an EP. Furthermore, it shows that when fluctuation effects are considered, the SNR of any reciprocal system is fundamentally constrained, regardless of its use of EPs. These insights critically address the limitations of EP-based sensing, shifting the focus from EP proximity to more significant factors such as nonreciprocal interactions and gain in the system dynamics.

Instead of relying on eigenmode coalescence at EPs, singularity-tuned systems take advantage of internal parameter tuning that amplifies response to perturbations – a sensitivity boost that differs fundamentally from that of EP-based systems [22, 24]. This divergence is related to proximity to a dynamical phase transition, which has recently been recognized as a valuable resource in quantum sensing. Unlike the more conventional amplification methods, this approach benefits from the unique properties of singularities in the non-Hermitian space, creating a form of criticality-enhanced sensitivity that is robust under a wider range of noise conditions than EP-based systems [27–31].

In [24], it was demonstrated that in a two-mode bosonic system, the error $\delta\theta$ in estimating a parameter θ scales as $\delta\theta \propto \theta^s$, where s corresponds to the order of the pole in the singular response function. Notably, when the parameter affects the common frequency and the singularity arises from satisfying the EP condition, the error exhibits *quadratic* scaling. This work extends the previous analysis by generalizing it to a four-mode cavity system featuring both a second-order EP and a second-order DP. We demonstrate that quadratic scaling persists at the second-order EP, even when an orthogonal subspace emerges due to the second-order DP. In the system under consideration, satisfying both the EP condition and the singularity condition of the dynamical generator necessitates meeting the diabolic condition. As a result, enhanced precision is observed specifically at HED points.

The structure of this paper is as follows: Section II provides a concise overview of the classical Fisher information and its

*Electronic address: javid.naikoo@amu.edu.pl

quantum counterpart, the quantum Fisher information, emphasizing their critical roles in estimation theory. Section III presents a comprehensive description of a sensor model, including the mathematical framework for Gaussian estimation of linear perturbations within this context. The primary results of this study are discussed in Sec. IV, where we analyze the sensing advantages at HEP singularities. Finally, the conclusions are summarized in Sec. V.

II. FUNDAMENTAL BOUNDS ON PARAMETER ESTIMATION: THE ROLE OF FISHER INFORMATION

The Fisher information and the Cramér-Rao bound are foundational concepts in estimation theory, quantifying the limits of precision in parameter estimation. These concepts are pivotal in both classical and quantum domains, offering insight into the optimal accuracy achievable under the constraints of measurement and inherent noise.

A. Classical Fisher Information and the Cramér-Rao Bound

In classical statistics, Fisher information provides a measure of the sensitivity of a probability distribution to the changes in a parameter. For a probability distribution $p(x|\theta)$ that depends on an unknown parameter θ , the Fisher information F_θ is defined as

$$F_\theta = \mathbb{E} \left[\left(\frac{\partial}{\partial \theta} \log p(x|\theta) \right)^2 \right], \quad (1)$$

where \mathbb{E} denotes the expectation over the variable x sampled from $p(x|\theta)$. Intuitively, a higher Fisher information value indicates that small changes in θ lead to larger variations in the probability distribution, suggesting that θ can be estimated with higher precision.

The Cramér-Rao bound establishes a lower bound on the variance of any unbiased estimator $\hat{\theta}$ of the parameter θ , providing a measure of the best possible accuracy achievable in estimating θ under unbiased conditions. For an unbiased estimator, the classical Cramér-Rao bound is given by:

$$\delta^2(\hat{\theta}) \geq \frac{1}{F_\theta}, \quad (2)$$

where $\delta^2(\hat{\theta})$ denotes the variance of $\hat{\theta}$. This inequality implies that the inverse of the Fisher information is the lowest achievable variance for any unbiased estimator, setting a theoretical limit on estimation precision.

B. Quantum Fisher Information and the Quantum Cramér-Rao Bound

In quantum mechanics, the Fisher information concept extends to account for the intrinsic probabilistic nature of quantum measurements. Quantum Fisher information (QFI)

characterizes how sensitively the state of a quantum system changes with respect to a parameter θ , taking into account both the probabilistic nature of measurement outcomes and the underlying quantum state dynamics.

Consider a quantum state $\rho(\theta)$ that depends on the parameter θ . The QFI \mathcal{F}_θ for this state is defined as

$$\mathcal{F}_\theta = \text{Tr} [\rho(\theta) L_\theta^2], \quad (3)$$

where L_θ is the symmetric logarithmic derivative (SLD) operator, implicitly defined by the equation:

$$\frac{\partial \rho(\theta)}{\partial \theta} = \frac{1}{2} \left[L_\theta \rho(\theta) + \rho(\theta) L_\theta \right]. \quad (4)$$

The SLD, L_θ , serves as a quantum analog to the derivative of the log-likelihood function in the classical case, capturing how changes in θ affect the quantum state. The QFI is crucial in fields such as quantum metrology, where it enables the design of measurement protocols that maximize parameter estimation precision under quantum mechanical constraints.

The precision limits imposed by the QFI are formalized by the *quantum Cramér-Rao bound*, which sets a fundamental limit on the variance of any unbiased estimator $\hat{\theta}$ for the parameter θ . The quantum Cramér-Rao bound states that $\delta^2(\hat{\theta}) \geq \frac{1}{\mathcal{F}_\theta}$ and satisfies

$$\delta^2(\hat{\theta}) \geq \frac{1}{F_\theta} \geq \frac{1}{\mathcal{F}_\theta}. \quad (5)$$

This bound indicates that the inverse of the QFI is the minimum achievable variance, setting an ultimate limit on precision that is attainable by optimizing both measurement and quantum state preparation.

In practical terms, the quantum Cramér-Rao bound plays a central role in quantum sensing and metrology, guiding the development of quantum-enhanced measurement strategies that leverage entanglement, coherence, and other uniquely quantum properties to surpass classical precision limits. By carefully engineering quantum states and measurements to maximize \mathcal{F}_θ , it is possible to achieve higher sensitivity in estimating parameters such as phase, frequency, and other physical quantities of interest in quantum systems.

III. SENSOR MODEL: A BOSONIC SYSTEM WITH HYBRID EXCEPTIONAL AND DIABOLIC POINTS

Let us consider a system of four bosonic modes \hat{a}_ℓ $\ell = 1, \dots, 4$, described by the following Hamiltonian

$$\begin{aligned} \hat{H}_S = & \sum_{\ell=1}^4 \omega_\ell \hat{a}_\ell^\dagger \hat{a}_\ell + g(\hat{a}_1^\dagger \hat{a}_2 + \hat{a}_3^\dagger \hat{a}_4 + \text{h.c.}) \\ & + J(\hat{a}_1^\dagger \hat{a}_3 + \hat{a}_2^\dagger \hat{a}_4 + \text{h.c.}). \end{aligned} \quad (6)$$

We assume that the odd-numbered modes, \hat{a}_1, \hat{a}_3 and the even-numbered modes, \hat{a}_2, \hat{a}_4 experience loss and gain, respectively. This loss-gain dynamics can be modeled through

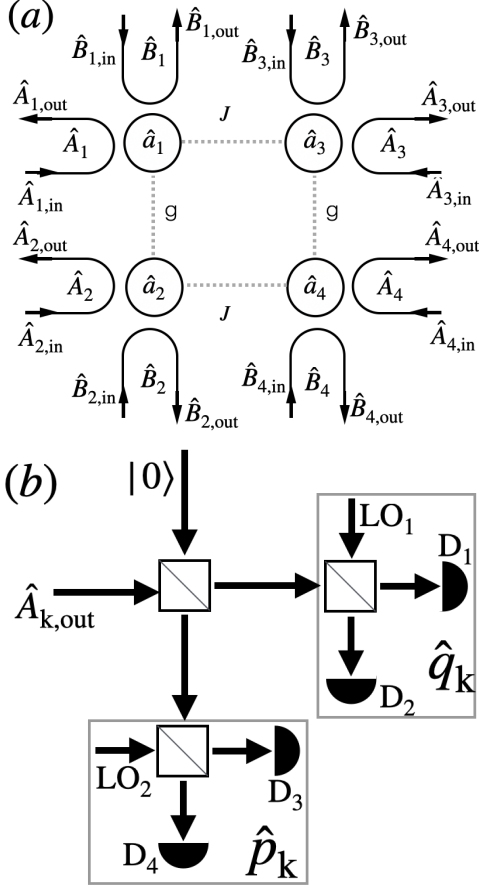


Figure 1: (a) **Sensor model** of four bosonic modes \hat{a}_k interacting with *inaccessible* bath modes \hat{B}_k through dissipative (for $k=1, 3$) and amplification (for $k=2, 4$) interactions. All the four cavity modes are probed by *accessible* (Gaussian) input field \hat{A}_k via dissipative interaction. Using input-output formalism, the accessible and the inaccessible field modes are expressed in terms of the input and output fields ($\hat{A}_{k,\text{in/out}}$ and $\hat{B}_{k,\text{in/out}}$) as defined in Eq. (10). (b) **Heterodyne detection**, which is equivalent to double *homodyne* detection, is performed on the outputs from the accessible modes i.e. $\hat{A}_{k,\text{out}}$, by combining them with the vacuum $|0\rangle$ on a balanced beam splitter. The resulting fields are then mixed with local oscillators (LO_1 and LO_2) on two additional balanced beam splitters. The outputs from these are measured by detectors (D_k) to determine the quadratures \hat{p}_k and \hat{q}_k .

the following interactions:

$$H_{\text{int,odd}} = \sum_{\ell=\text{odd}} \int_{-\infty}^{\infty} d\omega' \sqrt{\frac{\eta_{\ell}(\omega')}{2\pi}} [\hat{a}_{\ell} \hat{B}_{\ell}^{\dagger}(\omega') + \text{h.c.}], \quad (7)$$

$$H_{\text{int,even}} = \sum_{\ell=\text{even}} \int_{-\infty}^{\infty} d\omega' \sqrt{\frac{\eta_{\ell}(\omega')}{2\pi}} [\hat{a}_{\ell}^{\dagger} \hat{B}_{\ell}(\omega') + \text{h.c.}]. \quad (8)$$

Here, the bath mode operators $\hat{B}_{1(3)}$ and $\hat{B}_{2(4)}$ are responsible for the *intrinsic* loss and gain in the cavity modes $\hat{a}_{1(3)}$ and the mode $\hat{a}_{2(4)}$, respectively. Further, we allow each cavity mode \hat{a}_{ℓ} to be probed by a controllable field \hat{A}_{ℓ} and such probing

introduces further loss to each cavity mode \hat{a}_{ℓ} modeled by the following interaction

$$H_{\text{int,probe}} = \sum_{\ell=1}^4 \int_{-\infty}^{\infty} d\omega' \sqrt{\frac{\kappa(\omega')}{2\pi}} [\hat{a}_{\ell} \hat{A}_{\ell}^{\dagger}(\omega') + \text{h.c.}]. \quad (9)$$

The auxiliary field modes \hat{A}_{ℓ} and \hat{B}_{ℓ} with $\ell = 1, \dots, 4$ individually satisfy the usual bosonic commutation relations $[A_{\ell}(\omega'), A_{\ell}^{\dagger}(\omega'')] = [B_{\ell}(\omega'), B_{\ell}^{\dagger}(\omega'')] = \delta(\omega' - \omega'')$. For each optical mode, $\hat{O}_{\ell,\omega'} \in \{\hat{A}_{\ell,\omega'}, \hat{B}_{\ell,\omega'}\}$, we define its effective input and output field as

$$\begin{aligned} \hat{O}_{\ell,\text{in}}(t) &:= -\frac{i}{\sqrt{2\pi}} \int_{-\infty}^{\infty} d\omega' \hat{O}_{\ell,\omega'}(t_i) e^{-i\omega'(t-t_i)}, \\ \hat{O}_{\ell,\text{out}}(t) &:= -\frac{i}{\sqrt{2\pi}} \int_{-\infty}^{\infty} d\omega' \hat{O}_{\ell,\omega'}(t_f) e^{-i\omega'(t-t_f)}, \end{aligned} \quad (10)$$

which satisfy $[\hat{O}_{\ell,\text{in/out}}(t), \hat{O}_{\ell,\text{in/out}}(t')^{\dagger}] = \delta(t - t')$ and lead to the following input-output relation [32]

$$\hat{O}_{\ell,\text{out}}(t) = \hat{O}_{\ell,\text{in}}(t) - \sqrt{\kappa} \hat{a}_{\ell}(t). \quad (11)$$

Assuming all the cavity modes to be of same frequency $\omega_{\ell} =: \omega_0 \forall \ell = 1, \dots, 4$, the cavity mode vector $\hat{\mathbf{a}} := (\hat{a}_1, \hat{a}_2, \hat{a}_3, \hat{a}_4)^T$ obeys the following Langevin equation [7, 9, 10, 24, 33, 34]:

$$\partial_t \hat{\mathbf{a}} = -i(\omega_0 \mathbf{I} + \mathbf{H}) \hat{\mathbf{a}} + \mathbf{K}_{\text{probe}} \hat{\mathbf{A}}_{\text{in}} + \mathbf{K}_{\text{diss}} \hat{\mathbf{B}}_{\text{in}} + \mathbf{K}_{\text{amp}} \hat{\mathbf{B}}_{\text{in}}^{\dagger}, \quad (12)$$

where

$$\mathbf{H} = \begin{pmatrix} -i\gamma_1 & g & J & 0 \\ g & i\gamma_2 & 0 & J \\ J & 0 & -i\gamma_3 & g \\ 0 & J & g & i\gamma_4 \end{pmatrix}, \quad (13)$$

and $\gamma_1 = (\eta_1 + \kappa)/2$, $\gamma_2 = (\eta_2 - \kappa)/2$, $\gamma_3 = (\eta_3 + \kappa)/2$ and $\gamma_4 = (\eta_4 - \kappa)/2$. The input vectors as defined in Eq. (10) are $\hat{\mathbf{A}}_{\text{in}} = (\hat{A}_{1,\text{in}} \hat{A}_{2,\text{in}} \hat{A}_{3,\text{in}} \hat{A}_{4,\text{in}})^T$, $\hat{\mathbf{B}}_{\text{in}} = (\hat{B}_{1,\text{in}} \hat{B}_{2,\text{in}} \hat{B}_{3,\text{in}} \hat{B}_{4,\text{in}})^T$, $\hat{\mathbf{B}}_{\text{in}}^{\dagger} = (\hat{B}_{1,\text{in}}^{\dagger} \hat{B}_{2,\text{in}}^{\dagger} \hat{B}_{3,\text{in}}^{\dagger} \hat{B}_{4,\text{in}}^{\dagger})^T \neq (\hat{\mathbf{B}}_{\text{in}})^{\dagger}$. The various coupling matrices are $\mathbf{K}_{\text{probe}} = \text{diag}(\sqrt{\kappa}, \sqrt{\kappa}, \sqrt{\kappa}, \sqrt{\kappa})$, $\mathbf{K}_{\text{diss}} = \text{diag}(\sqrt{\eta_1}, 0, \sqrt{\eta_3}, 0)$, $\mathbf{K}_{\text{amp}} = \text{diag}(0, -\sqrt{\eta_2}, 0, -\sqrt{\eta_4})$.

Up to this point, we have assumed that all system parameters are fixed and known. However, in realistic scenarios, certain parameters might be subject to small variations or uncertainties. To capture this, we now introduce a *linear* perturbation parameter θ , which is encoded within the system's dynamical generator \mathbf{H} given in Eq. (13). The resulting perturbed generator, denoted by \mathbf{H}_{θ} , takes the following form

$$\mathbf{H}_{\theta} = \mathbf{H} - \theta \mathbf{n}. \quad (14)$$

Here, \mathbf{n} is the perturbation matrix that specifies which parameters in the system are affected by the perturbation. This matrix

allows us to control the sensitivity of the system dynamics to changes in θ .

For instance, if we set $\mathbf{n} = \mathbf{I}$, where \mathbf{I} is the identity matrix, then the perturbation parameter θ influences the common cavity frequency, ω_0 . This configuration implies that θ shifts the entire frequency spectrum by a small amount, modeling a uniform frequency perturbation across all modes. In more general cases, \mathbf{n} could represent specific structures, allowing targeted perturbations to certain elements of \mathbf{H} , such as coupling strengths, decay rates, or detuning parameters.

Through this approach, we can analyze the robustness of the system's behavior under small parameter shifts and explore how different choices of \mathbf{n} impact the dynamics induced by the perturbed generator \mathbf{H}_θ .

A. Solution in the Fourier space

At this point, it is useful to transform Eq. (12) into the Fourier space by defining the Fourier transform of a time-dependent operator $\hat{\mathbf{u}}(t) = (\hat{u}_1(t) \ \hat{u}_2(t) \ \dots)^T$ as $\hat{\mathbf{u}}[\omega] := \mathcal{F}_\omega[\hat{\mathbf{u}}(t)] = \int dt e^{i\omega t} \hat{\mathbf{u}}(t)$. The correspondent position and momentum quadratures are defined as $\hat{q}^u[\omega] = \hat{\mathbf{u}}[\omega] + (\hat{\mathbf{u}}[\omega])^\dagger$ and $i\hat{p}^u[\omega] = \hat{\mathbf{u}}[\omega] - (\hat{\mathbf{u}}[\omega])^\dagger$. Thus, Eq. (12) in the Fourier space reads:

$$-i\omega \hat{\mathbf{a}}[\omega] = -i(\omega_0 \mathbf{I} + \mathbf{H}) \hat{\mathbf{a}}[\omega] + \mathbf{K}_{\text{probe}} \hat{\mathbf{A}}_{\text{in}}[\omega] + \mathbf{K}_{\text{diss}} \hat{\mathbf{B}}_{\text{in}}[\omega] + \mathbf{K}_{\text{amp}} \hat{\mathbf{B}}_{\text{in}}^\dagger[\omega]. \quad (15)$$

Since we will be working with Gaussian probe fields, which are completely characterized by amplitude and covariance matrix, we define the quadratures vectors corresponding to the cavity modes $\hat{\mathbf{S}}^S[\omega] := (\hat{q}_1[\omega], \dots, \hat{q}_4[\omega], \hat{p}_1[\omega], \dots, \hat{p}_4[\omega])^T$, as well as the auxiliary field modes $\hat{\mathbf{S}}_{\text{in}}^\bullet[\omega] := (\hat{q}_1^{\bullet \text{in}}[\omega], \dots, \hat{q}_4^{\bullet \text{in}}[\omega], \hat{p}_1^{\bullet \text{in}}[\omega], \dots, \hat{p}_4^{\bullet \text{in}}[\omega])^T$, and $\bullet = A, B$. In this quadrature representation Eq. (15) becomes

$$-\omega \mathbf{J} \hat{\mathbf{S}}^S[\omega] = -(\omega_0 \mathbf{I} + \mathbf{H}) \mathbf{J} \hat{\mathbf{S}}^S[\omega] + \sqrt{\kappa} \hat{\mathbf{S}}_{\text{in}}^A[\omega] + \mathbf{K}_{B_1} \hat{\mathbf{S}}_{\text{in}}^B[\omega] + \mathbf{K}_{B_2} \hat{\mathbf{S}}_{\text{in}}^B[-\omega]. \quad (16)$$

In the context of Eq. (15), any (4×4) matrix \mathbf{F} is now expressed in the (symplectic) phase space as

$$\mathbf{F} \equiv \mathcal{J}\{\mathbf{F}\} := \begin{pmatrix} \text{Re}[\mathbf{F}] & -\text{Im}[\mathbf{F}] \\ \text{Im}[\mathbf{F}] & \text{Re}[\mathbf{F}] \end{pmatrix}, \quad (17)$$

so that $\mathbf{H} = \mathcal{J}\{\mathbf{H}\}$, $\mathbf{I} = \mathcal{J}\{\mathbf{I}\}$ corresponds to a 8×8 identity matrix, and $\mathbf{J} = \mathcal{J}\{i\mathbf{I}\}$ is the symplectic form, which plays the role of the imaginary unit. Similarly, the input output relation in Eq. (11) is given in quadrature basis by

$$\hat{\mathbf{S}}_{\text{out}}^A[\omega] = \hat{\mathbf{S}}_{\text{in}}^A[\omega] - \sqrt{\kappa} \hat{\mathbf{S}}_{\text{in}}^S[\omega]. \quad (18)$$

Using Eq. (16) together with Eq. (18), we have

$$\hat{\mathbf{S}}_{\text{out}}^A[\omega] = (\mathbf{I} - \mathbf{K}_{\text{probe}} \mathbf{G}[\omega]) \hat{\mathbf{S}}_{\text{in}}^A[\omega] - \mathbf{K}_{\text{probe}} \mathbf{G}[\omega] \left(\mathbf{K}_{\text{diss}} \hat{\mathbf{S}}_{\text{in}}^B[\omega] + \mathbf{K}_{\text{amp}} \hat{\mathbf{S}}_{\text{in}}^B[-\omega] \right), \quad (19)$$

where the coupling matrices are given by $\mathbf{K}_{\text{probe}} = \text{diag}(\mathbf{K}_{\text{probe}}, \mathbf{K}_{\text{probe}})$, $\mathbf{K}_{\text{diss}} = \text{diag}(\mathbf{K}_{\text{diss}}, \mathbf{K}_{\text{diss}})$ and $\mathbf{K}_{\text{amp}} = \text{diag}(\mathbf{K}_{\text{amp}}, -\mathbf{K}_{\text{amp}})$, and $\mathbf{G}[\omega]$ is the system's response function

$$\mathbf{G}[\omega] = \mathbf{J} \left((\omega - \omega_0) \mathbf{I} - \mathbf{H} \right)^{-1}. \quad (20)$$

We can further simplify Eq. (19) as

$$\hat{\mathbf{S}}_{\text{out}}^A[\omega] = (\mathbf{I} - \mathbf{K}_{\text{probe}} \mathbf{G}[\omega]) \hat{\mathbf{S}}_{\text{in}}^A[\omega] - \mathbf{K}_{\text{probe}} \mathbf{G}[\omega] \mathcal{K} \hat{\mathbf{S}}^B[\pm\omega], \quad (21)$$

where \mathcal{K} is an 8×16 matrix given in block form by $\mathcal{K} = [\mathbf{K}_{\text{diss}}, \mathbf{0}, \mathbf{K}_{\text{amp}}, \mathbf{0}; \mathbf{0}, \mathbf{K}_{\text{diss}}, \mathbf{0}, \mathbf{K}_{\text{amp}}]$ and the vector $\hat{\mathbf{S}}^B[\pm\omega] = (\hat{q}_1^B[\omega] \cdots \hat{q}_4^B[\omega], \hat{q}_1^B[-\omega] \cdots \hat{q}_4^B[-\omega], \hat{p}_1^B[\omega] \cdots \hat{p}_4^B[\omega], \hat{p}_1^B[-\omega] \cdots \hat{p}_4^B[-\omega])^T$ include both positive and negative frequency components.

Let us define the average value $S := \langle \hat{S} \rangle$ and assume the auxiliary modes \hat{B}_ℓ to be in the vacuum state, so that $S_{\text{in}}[\omega]$ and $S_{\text{in}}[-\omega]$ vanish and from Eq. (21) we have

$$S_{\text{out}}^A[\omega] = (\mathbf{I} - \mathbf{K}_{\text{probe}} \mathbf{G}[\omega]) S_{\text{in}}^A[\omega]. \quad (22)$$

The covariance matrix of the output modes being measured, i.e. $\mathbf{V}_{\text{out}}^A[\omega]$ has elements $[\mathbf{V}_{\text{out}}^A]_{jk} = \frac{1}{2} \langle \{ [\hat{S}_{\text{out}}^A]_j, [\hat{S}_{\text{out}}^A]_k \} \rangle - \langle [\hat{S}_{\text{out}}^A]_j \rangle \langle [\hat{S}_{\text{out}}^A]_k \rangle$. It is not hard to show that an input-output relation, similar to Eq. (22), is given by [24]

$$\mathbf{V}_{\text{out}}^A[\omega] = (\mathbf{I} - \mathbf{K}_{\text{probe}} \mathbf{G}[\omega]) \mathbf{V}_{\text{in}}^A[\omega] (\mathbf{I} - \mathbf{K}_{\text{probe}} \mathbf{G}[\omega])^T + \mathbf{K}_{\text{probe}} \mathbf{G}[\omega] \mathcal{K} \tilde{\mathbf{V}}_{\text{in}}^B[\omega] \mathcal{K}^T \mathbf{G}[\omega]^T. \quad (23)$$

In what follows, we use the input covariance matrices

$$\mathbf{V}_{\text{in}}^A = (2n_A + 1) \mathbf{I}_{8 \times 8}, \quad \tilde{\mathbf{V}}_{\text{in}}^B = (2n_B + 1) \mathbf{I}_{16 \times 16}, \quad (24)$$

where n_A and n_B are the average thermal photons associated with the probe and bath modes, respectively.

The perturbation described in Eq. (14) translates in the Fourier space to the following

$$\mathbf{H}_\theta = \mathbf{H} - \theta \mathbf{n}, \quad (25)$$

where \mathbf{n} is the the matrix \mathbf{n} in the Fourier space given by Eq. (17). Consequently, the modified Green's function changes to $\mathbf{G}[\omega] = \mathbf{J}((\omega - \omega_0) \mathbf{I} + \theta \mathbf{n} - \mathbf{H})^{-1}$. If we further assume that the probe frequency is in resonance with the system frequency i.e. $\omega = \omega_0$, we have

$$\mathbf{G}_\theta[\omega = \omega_0] = \mathbf{J}(\theta \mathbf{n} - \mathbf{H})^{-1}. \quad (26)$$

As a result, the output amplitude in Eq. (22) and the covariance matrix in Eq. (23) depend on θ and we denote them as

$$S_{\text{out}}^A[\omega = \omega_0] \rightarrow S_{\text{out},\theta}^A, \quad \mathbf{V}_{\text{out}}^A[\omega = \omega_0] \rightarrow \mathbf{V}_{\text{out},\theta}^A. \quad (27)$$

We stress that the θ -parameter dependence of $S_{\text{out},\theta}^A$ and $\mathbf{V}_{\text{out},\theta}^A$ is entirely through the response function $\mathbf{G}_\theta[\omega = \omega_0]$ in Eq. (26).

B. Gaussian estimation of linear perturbations

Since we are focusing on Gaussian probe signals – the input bosonic modes $\hat{A}_{k,in}$ in Fig. 1, it is worth to briefly revisit the estimation theory with Gaussian states and Gaussian measurements [35, 36]. A Gaussian state $\rho(S, V)$ is completely characterized by its amplitude S and covariance matrix V . In the Gaussian estimation theory, an unknown parameter θ is encoded on these amplitude and covariance matrix resulting in a Gaussian state $\rho_\theta = \rho(S_\theta, V_\theta)$. The ultimate precision in estimating θ is then given by the QFI,

$$\mathcal{F}_\theta = \frac{1}{2} \text{Tr} \left[\frac{dV_\theta}{d\theta} V_\theta^{-1} \frac{dV_\theta}{d\theta} V_\theta^{-1} \right] + 2 \left(\frac{dS_\theta}{d\theta} \right)^T V_\theta^{-1} \left(\frac{dS_\theta}{d\theta} \right). \quad (28)$$

In the context of our model with the amplitude and covariance matrix given in Eq. (27), the QFI, as given in Eq. (28), reads

$$\mathcal{F}_\theta = \frac{1}{2} \text{Tr} \left[\frac{dV_{\text{out},\theta}^A}{d\theta} (V_{\text{out},\theta}^A)^{-1} \frac{dV_{\text{out},\theta}^A}{d\theta} (V_{\text{out},\theta}^A)^{-1} \right] + 2 \left(\frac{dS_{\text{out},\theta}^A}{d\theta} \right)^T (V_{\text{out},\theta}^A)^{-1} \left(\frac{dS_{\text{out},\theta}^A}{d\theta} \right). \quad (29)$$

One can use this formula directly to determine precision by fixing system parameters H and choosing a desired perturbation matrix n . It is worth mentioning that the QFI is an optimized quantity which is obtained by maximizing the classical Fisher information over all possible measurements [37]. It is important to ask if a specific measurement strategy saturates the precision obtained by QFI. As it is described in the next section, the *heterodyne* detection performed on the output signals is the optimal measurement for our system. Such a detection leads to a probability distribution $p(x_\theta)$ where x_θ is a vector of (real) measurement outcomes. In the context of our bosonic system, the distribution reads

$$p(x_\theta) = \frac{1}{(2\pi)^N \sqrt{C_\theta}} \exp \left(-\frac{1}{2} (x_\theta - \bar{x})^T C_\theta^{-1} (x_\theta - \bar{x}) \right), \quad (30)$$

where

$$x_\theta = S_{\text{out},\theta}^A, \quad C_\theta = V_{\text{out},\theta}^A + I, \quad (31)$$

is the amplitude and covariance matrix and the Fisher information is accordingly given by [38]

$$F_\theta = \frac{1}{2} \text{Tr} \left[\frac{dC_\theta}{d\theta} C_\theta^{-1} \frac{dC_\theta}{d\theta} C_\theta^{-1} \right] + 2 \left(\frac{dx_\theta}{d\theta} \right)^T C_\theta^{-1} \left(\frac{dx_\theta}{d\theta} \right). \quad (32)$$

Singular dynamical generator

So far, we have laid the groundwork by showing that the precision (or QFI) can be computed through a straightforward

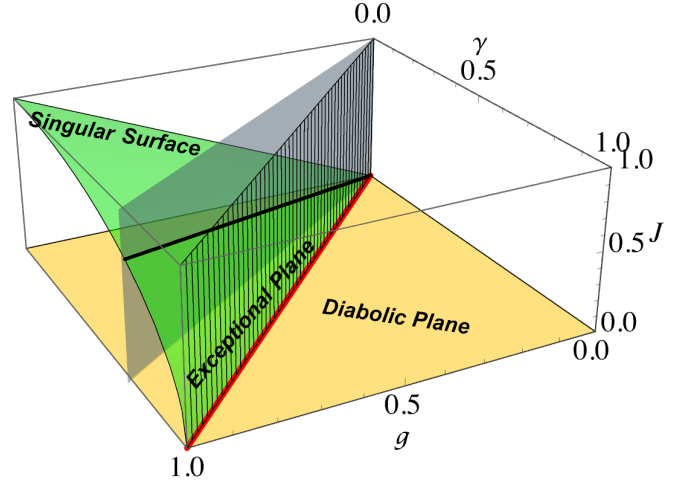


Figure 2: **Parameter space of the dynamical generator H in Eq. (13)** with balanced gain and loss $\gamma_\ell = \gamma$ for all $\ell = 1, \dots, 4$. Here, J represents the coupling between successive modes with gain or loss, and g is the coupling strength between a loss mode $\hat{a}_{1(3)}$ and a gain mode $\hat{a}_{2(4)}$. The green surface, denoted as *singular surface*, shows points where $J = \sqrt{g^2 - \gamma^2}$, where H becomes *singular* (denoted by H_S) as given in Eq. (42). The yellow horizontal plane $J = 0$ contains *diabolic points*, while the vertical meshed plane $g = \gamma$ includes *exceptional points*. The intersection of singular surface, the exceptional plane and the diabolic plane is given by the hybrid exceptional-diabolic (HED) line in red. The gray plane at $g = \sqrt{2}\gamma$ is an arbitrary non-EP plane that intersects the singularity surface along the black line. The singular points along red (HEP) and black (non-HEP or non-EP) lines exhibit distinct scaling types of behavior as shown in Fig. 3 by red and black curves, respectively.

formula (29) involving the amplitude and covariance matrix. We are now prepared to explore the effect of the nature of the dynamical generator, denoted by H (or equivalently H), on this precision. The precision is influenced by H via the response function G in Eq. (26), which serves as the central object of our analysis. Two distinct cases emerge:

Non-singular dynamical generator.— When H in Eq. (26) [or equivalently H in Eq. (13)] is invertible, the Neumann series can be applied to obtain

$$G_\theta[\omega = \omega_0] = J(\theta H_\theta - H)^{-1} = -JH^{-1} \sum_{k=0}^{\infty} (\theta n_\theta H^{-1})^k, \quad (33)$$

which approaches $(-JH^{-1})$ as $\theta \rightarrow 0$. Using this in Eq. (29), the QFI turns out to be

$$\mathcal{F}_\theta = a_0 + \mathcal{O}(\theta), \quad a_0 \neq 0, \quad (34)$$

indicating that the leading-order term is independent of θ . Here, we have

$$a_0 = \frac{1}{2} \text{Tr} [Y^{-1} Z Y^{-1} Z] + 2\kappa^2 S_{\text{in}}^T g_1^T Y^{-1} g_1 S_{\text{in}}, \quad (35)$$

where

$$Y = V_{\text{in}}^A - \kappa(g_0 V_{\text{in}}^A + V_{\text{in}}^A g_0^T) + g_0 \Lambda g_0^T, \quad (36)$$

$$Z = -\kappa(g_1 V_{\text{in}}^A + V_{\text{in}}^A g_1^T) + g_0 \Lambda g_1^T + g_1 \Lambda g_0^T, \quad (37)$$

$$\Lambda = \kappa^2 V_{\text{in}}^A + \kappa \mathcal{K}(V_{B_1} \oplus V_{B_2}) \mathcal{K}^T, \quad (38)$$

with $g_k = -\mathbf{J}\mathbf{H}(\mathbf{n}\mathbf{H}^{-1})^k$ for $k = 0, 1$ [24].

Singular dynamical generator.— Conversely, when \mathbf{H} is non-invertible, or *singular*, the inverse of Eq. (26) can be calculated using the Sain-Massey expansion from singular matrix perturbation theory [39, 40], yielding

$$\begin{aligned} G_\theta[\omega = \omega_0] &= \mathbf{J}(\theta\mathbf{n} - \mathbf{H}_S)^{-1} \\ &= \theta^{-s} [\mathbf{X}_0 + \theta\mathbf{X}_1 + \theta^2\mathbf{X}_2 + \dots], \end{aligned} \quad (39)$$

where $\mathbf{X}_0 \neq 0$, and s is an integer that determines the pole order in this expansion (see Appendix B). In this scenario, the QFI in Eq. (28) exhibits a divergent behavior,

$$\mathcal{F}_\theta = \theta^{-2s} [b_0 + \mathcal{O}(\theta)], \quad b_0 \neq 0, \quad (40)$$

where the coefficient is given by [24]

$$\begin{aligned} b_0 &= \text{Tr}(\mathbf{n}\mathbf{X}_0\mathbf{n}\mathbf{X}_0 + \mathbf{V}_{\text{in}}^{-1}\mathbf{n}\mathbf{X}_0\mathbf{V}_{\text{in}}\mathbf{X}_0^T\mathbf{n}^T) \\ &+ \kappa^2\mathbf{S}_{\text{in}}^T\mathbf{X}_0^T\mathbf{n}^T\mathbf{V}_{\text{in}}^{-1}\mathbf{n}\mathbf{X}_0\mathbf{S}_{\text{in}}. \end{aligned} \quad (41)$$

The above analysis reveals that the nature of the dynamical generator \mathbf{H} critically affects the behavior of the QFI and, consequently, the achievable precision in parameter estimation. In essence, the nature of the dynamical generator \mathbf{H} —whether singular or non-singular—determines the balance between stable precision and enhanced sensitivity in parameter estimation. For non-singular \mathbf{H} , the QFI remains finite as $\theta \rightarrow 0$, ensuring consistent precision and resilience to small perturbations, which supports stable measurement outcomes. Conversely, when \mathbf{H} is singular, the QFI diverges as $\theta \rightarrow 0$, allowing for high sensitivity to parameter variations. This distinction enables the design of quantum systems tailored for either stable precision or heightened sensitivity, aligning experimental goals with the nature of \mathbf{H} .

IV. ENHANCED PRECISION AT HYBRID EXCEPTIONAL-DIABOLIC POINTS

Let us first take a quick look at the structure of the dynamical generator \mathbf{H} in Eq. (13). If we assume all the gain and loss rates are equal i.e. $\gamma_\ell = \gamma, \forall \ell = 1, 2, 3, 4$, the matrix \mathbf{H} can be expressed as direct sum $\mathbf{H} = \mathbf{M}_1 \otimes \mathbf{I} + \mathbf{I} \otimes \mathbf{M}_2$ where $\mathbf{M}_1 = [0, J; J, 0]$ and $\mathbf{M}_2 = [-i\gamma, g; g, i\gamma]$ with eigenvalues $\lambda_{1,\pm} = \pm J$ and $\lambda_{2,\pm} = \pm\sqrt{g^2 - \gamma^2}$, respectively [8]. Such a decomposition is useful since the eigenvalues of \mathbf{H} , denoted by $\mu_{k,\ell,\pm} = \lambda_{k,\pm} + \lambda_{\ell,\pm}$ with $k, \ell = 1, 2$, are simply given by the sum of the eigenvalues of \mathbf{M}_1 and \mathbf{M}_2 . Secondly, \mathbf{H} demonstrates an exceptional curve when $g = \gamma$ for all points $\mu_{k,\ell,\pm} = \pm J$ while as for $J = 0$ pertains to a diabolic curve given by all points $\mu_{k,\ell,\pm} = \pm\sqrt{g^2 - \gamma^2}$. However, what is going to be an even more interesting case for us is that \mathbf{H} is singular for all points satisfying $J = \pm\sqrt{g^2 - \gamma^2}$ and we denote it as follows (restricting to positive square root)

$$\mathbf{H}_S = \begin{pmatrix} -i\gamma & g & \sqrt{g^2 - \gamma^2} & 0 \\ g & i\gamma & 0 & \sqrt{g^2 - \gamma^2} \\ \sqrt{g^2 - \gamma^2} & 0 & -i\gamma & g \\ 0 & \sqrt{g^2 - \gamma^2} & g & i\gamma \end{pmatrix}. \quad (42)$$

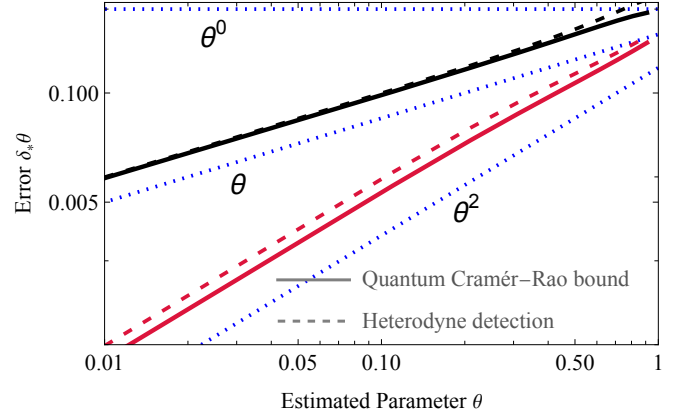


Figure 3: **Estimation error of the parameter θ** affecting cavity frequency ω_0 in Eq. (12). The solid curves correspond to the quantum Cramér-Rao bound $\delta_Q\theta = 1/\sqrt{\mathcal{F}_\theta}$, where \mathcal{F}_θ is numerically calculated from Eq. (29). The dashed curves represent the classical Cramér-Rao bound achieved through heterodyne detection, expressed as $\delta_C\theta = 1/\sqrt{F_\theta}$ with F_θ obtained numerically from Eq. (32). The scaling depicted by the quantum Cramér-Rao bound in the two cases is in agreement with the analytic results given in Eqs. (46) and (50). Similarly analytic predictions are obtained for heterodyne detection. The dotted blue lines serve as reference lines, scaling proportionally to θ and θ^2 , as indicated. The quadratic error scaling exhibited by the red solid and dashed curves is achieved by tuning the singular generator \mathbf{H}_S in Eq. (42) to $g = \gamma$, corresponding to the HED line in the parameter space shown in Fig. 2. In contrast, the black solid and dashed curves indicate linear scaling, where the singular generator \mathbf{H}_S is set to $g = \sqrt{2}\gamma$, representing the non-HED black line in Fig. 2. The parameters used include a common loss/gain rate γ set to $\gamma = 1$, coupling strengths $\kappa = 1$, $\eta_1 = \eta_2 = \eta_3 = \eta_4 = 0.5$. The average number of thermal photons in the input Gaussian probe and the bath is set to $n_A = n_B = 1$.

In light of the discussion in Sec. III B, one expects enhanced sensitivity in sensing linear perturbations when the system is operator at \mathbf{H}_S . However, note that in Sec. III B, the conclusion about enhanced precision was based on the singularity \mathbf{H} and not of \mathbf{H} . However, it turns out that $\det \mathbf{H} = |\det \mathbf{H}|^2$ (see Lemma 2 in the supplementary material of [24]). Therefore, in light of Eq. (17), $\mathbf{H}_S = \mathcal{J}\{\mathbf{H}_S\}$ is also singular and the expansion Eq. (39) applies.

The precision enhancement is quantified in terms of the pole order s in the expansion Eq. (39) – which for a particular \mathbf{H}_S is determined by the perturbation matrix \mathbf{n} . Let us consider the as an example the perturbation matrix $\mathbf{n} = \mathbf{I}$ – an 8×8 identity matrix. This matrix perturbs the common cavity frequency ω_0 by the same amount θ as $(\omega_0 - \theta)$.

Sensing at an HED singularity.— Let us consider the case when $g = \gamma$ i.e. the system is at HED point. Following the procedure in [24, 39] we find that the response function in Eq. (39) has the following form

$$G_\theta[\omega = \omega_0] = \theta^{-2}(\mathbf{X}_0 + \theta\mathbf{X}_1), \quad (43)$$

where

$$\mathbf{X}_0 = \mathbf{H}_S|_{g=\gamma}, \quad \mathbf{X}_1 = \mathbf{I}. \quad (44)$$

We can now use the response function $G_\theta[\omega = \omega_0]$ given by

Singularity Region	Condition	Sensitivity ($\delta_Q\theta, \delta_C\theta$)
Singular Surface	$J^2 = g^2 - \gamma^2$	θ ($g \neq \gamma$), θ^2 ($g = \gamma$)
Diabolical Plane	$J = 0$	θ^0 if $g \neq \gamma$
Exceptional Plane	$g = \gamma$	θ^0 if $J \neq 0$
HED Line	$(g, \gamma, J) = (\gamma, \gamma, 0)$	θ^2

Table I: **Summary of singularity types**, their corresponding conditions, and their relevance to the sensing parameter θ , which influences the common mode frequency. The sensitivity is quantified by the quantum and classical Cramér-Rao bounds, represented as $\delta_Q\theta = 1/\mathcal{F}_\theta$ and $\delta_C\theta = 1/F_\theta$, where \mathcal{F}_θ and F_θ denote the quantum and classical (pertaining to heterodyne detection) Fisher information, as provided in Eqs. (29) and (32), respectively.

Eq. (43) to calculate the corresponding amplitude and covariance matrix given in Eq. (22) and Eq. (23), respectively. Subsequently, we use these quantities to calculate the QFI given in Eq. (29) and obtain

$$\mathcal{F}_\theta^{\text{HED}} = \theta^{-4} [b'_0 + \mathcal{O}(\theta)], \quad (45)$$

where b'_0 is b_0 given in Eq. (41) for this particular case i.e. with perturbation matrix $n = 1$ and coefficient X_0 and X_1 given in Eq. (44). The precision in Eq. (45) leads to quadratic scaling of the error

$$\delta_Q\theta = \frac{1}{\sqrt{\mathcal{F}_\theta^{\text{HED}}}} \propto \theta^2. \quad (46)$$

Sensing at a non-HEP singularity.— Next, let us consider a non-HEP singularity by setting $g = \sqrt{2}\gamma$ in Eq. (42) [or equivalently in its quadrature representation $H_S(g, \gamma)$], we find

$$G_\theta[\omega = \omega_0] = \theta^{-1} [X_0 + \theta X_1 + \theta^2 X_2 + \dots], \quad (47)$$

where the even and odd coefficients are given by $X_{2k} = (2\gamma)^{-2k} X_{\text{even}}$ and $X_{2k+1} = (2\gamma)^{-2k-1} X_{\text{odd}}$

$$X_{\text{even}} = \begin{pmatrix} r^2 & 0 & 0 & r & 0 & 0 & -r^2 & 0 \\ 0 & r^2 & r & 0 & 0 & 0 & 0 & r^2 \\ 0 & r & r^2 & 0 & -r^2 & 0 & 0 & 0 \\ r & 0 & 0 & r^2 & 0 & r^2 & 0 & 0 \\ 0 & 0 & r^2 & 0 & r^2 & 0 & 0 & r \\ 0 & 0 & 0 & -r^2 & 0 & r^2 & r & 0 \\ r^2 & 0 & 0 & 0 & 0 & r & r^2 & 0 \\ 0 & -r^2 & 0 & 0 & r & 0 & 0 & r^2 \end{pmatrix},$$

$$X_{\text{odd}} = \begin{pmatrix} 0 & r & -r^2 & 0 & -r^2 & 0 & 0 & 0 \\ r & 0 & 0 & -r^2 & 0 & r^2 & 0 & 0 \\ -r^2 & 0 & 0 & r & 0 & 0 & -r^2 & 0 \\ 0 & -r^2 & r & 0 & 0 & 0 & 0 & r^2 \\ r^2 & 0 & 0 & 0 & 0 & r & -r^2 & 0 \\ 0 & -r^2 & 0 & 0 & r & 0 & 0 & -r^2 \\ 0 & 0 & r^2 & 0 & -r^2 & 0 & 0 & r \\ 0 & 0 & 0 & -r^2 & 0 & -r^2 & r & 0 \end{pmatrix}. \quad (48)$$

where $k = 0, 1, 2, \dots$ and $r = -1/\sqrt{2}$. Thus, in this case, the precision behaves as

$$\mathcal{F}_\theta^{\text{non-HED}} = \theta^{-2} [b''_0 + \mathcal{O}(\theta)], \quad (49)$$

with b''_0 being b_0 in Eq. (41) with coefficients given in Eq. (48). The form of precision in Eq. (49) leads to a linear scaling of the error

$$\delta_Q\theta = \frac{1}{\sqrt{\mathcal{F}_\theta^{\text{non-HED}}}} \propto \theta. \quad (50)$$

Consequently, while perturbing the system at the HED singularity achieves a quadratic scaling of error, perturbations away from this singularity result in only linear error scaling. These findings align with the numerical results shown in Fig. 3, which were obtained by directly computing the QFI from Eq. (28) without any approximations. For heterodyne detection, the CFI is given by Eq. (32) using the amplitude and covariance matrix specified in Eq. (31). By following the same procedure as outlined above, and analogous to Eqs. (45) and (49), the CFI in the two cases is obtained as:

$$F_\theta^{\text{HED}} = \theta^{-4} [c'_0 + \mathcal{O}(\theta)], \quad F_\theta^{\text{non-HED}} = \theta^{-2} [c''_0 + \mathcal{O}(\theta)], \quad (51)$$

where the coefficients $c'_0 > 0$ and $c''_0 > 0$. Consequently, the corresponding errors scale as:

$$\delta_C\theta = \frac{1}{\sqrt{F_\theta^{\text{HED}}}} \propto \theta^2, \quad \delta_C\theta = \frac{1}{\sqrt{F_\theta^{\text{non-HED}}}} \propto \theta. \quad (52)$$

The analytical predictions for the scaling behaviors in Eqs. (46), (50), and (52) are supported by the plots in Fig. 3, which were obtained by numerically computing the Fisher information given in Eqs. (29) and (32). A summary of the scaling behavior in different situations is presented in Table I.

V. CONCLUSION

In conclusion, our findings highlight the persistence of quadratic scaling at second-order EPs, even in the presence of orthogonal subspace induced by the second-order DPs in a four mode bosonic system. The interplay between EP condition, the singularity condition, and the diabolic condition of the dynamical generator is critical to achieving this enhanced precision. Notably, the quadratic scaling is uniquely observed at HED points, where these conditions naturally coalesce. This underscores the significance of HED points in optimizing precision and offers valuable insights for advancing non-Hermitian systems and quantum sensing applications. By using the tools of the singular matrix perturbation theory and Gaussian estimation framework, we reveal that HED points offer a significant twofold improvement in sensitivity over standard singularities in this system. The ultimate estimation limits, derived through the quantum Fisher information, identify heterodyne detection as the optimal measurement strategy to achieve this enhanced scaling. These results deepen our understanding of HED singularities and open pathways for their application in high-precision quantum sensing and metrology.

Acknowledgement

This work was supported by the Polish National Science Centre (NCN) under the Maestro Grant No. DEC-2019/34/A/ST2/00081. We thank Jan Kołodyński for insightful discussions.

Appendix A: Quantum Langevin Equations

The total Hamiltonian describing the sensor model in Fig. 1 reads

$$\hat{H} = \hat{H}_S + \hat{H}_B + \hat{H}_{SB}, \quad (\text{A1})$$

where

$$\begin{aligned} \hat{H}_S = & \sum_{\ell=1}^4 \omega_k \hat{a}_k^\dagger \hat{a}_k + g(\hat{a}_1^\dagger \hat{a}_2 + \hat{a}_3^\dagger \hat{a}_4 + \text{h.c.}) \\ & + J(\hat{a}_1^\dagger \hat{a}_3 + \hat{a}_2^\dagger \hat{a}_4 + \text{h.c.}), \end{aligned} \quad (\text{A2})$$

$$\begin{aligned} \hat{H}_B \approx & \sum_{\ell=1}^4 \int_{-\infty}^{\infty} d\omega' \omega' \hat{A}_\ell^\dagger(\omega') \hat{A}_\ell(\omega') \\ & + \sum_{\ell=1}^4 \int_{-\infty}^{\infty} d\omega' \omega' \hat{B}_\ell^\dagger(\omega') \hat{B}_\ell(\omega'), \end{aligned} \quad (\text{A3})$$

$$\begin{aligned} \hat{H}_{SB} \approx & \sum_{\ell=1}^4 \int_{-\infty}^{\infty} d\omega' \sqrt{\frac{\kappa(\omega')}{2\pi}} [\hat{a}_\ell \hat{A}_\ell^\dagger(\omega') + \text{h.c.}] \\ & + \sum_{\ell=2,4} \int_{-\infty}^{\infty} d\omega' \sqrt{\frac{\eta_\ell(\omega')}{2\pi}} [\hat{a}_\ell^\dagger \hat{B}_\ell^\dagger(\omega') + \text{h.c.}] \\ & + \sum_{\ell=1,3} \int_{-\infty}^{\infty} d\omega' \sqrt{\frac{\eta_\ell(\omega')}{2\pi}} [\hat{a}_\ell \hat{B}_\ell^\dagger(\omega') + \text{h.c.}], \end{aligned} \quad (\text{A4})$$

with commutation relations $[\hat{A}_\ell(\omega'), \hat{A}_\ell^\dagger(\omega'')] = [\hat{B}_\ell(\omega'), \hat{B}_\ell^\dagger(\omega'')] = \delta(\omega' - \omega'')$. The Heisenberg equation of motion $\partial_t \hat{\mathcal{O}} = -i[\hat{\mathcal{O}}, \hat{H}_{\text{total}}]$, where $\hat{H}_{\text{total}} = \hat{H}_S + \hat{H}_B + \hat{H}_{SB}$:

$$\partial_t \hat{a}_1 = -i\omega_1 \hat{a}_1 - ig_{12} \hat{a}_2 - iJ \hat{a}_3 - \hat{f}_1^A - \hat{f}_1^B, \quad (\text{A5})$$

$$\partial_t \hat{a}_2 = -i\omega_2 \hat{a}_2 - ig_{12} \hat{a}_1 - iJ \hat{a}_4 - \hat{f}_2^A - (\hat{f}_2^B)^\dagger, \quad (\text{A6})$$

$$\partial_t \hat{a}_3 = -i\omega_3 \hat{a}_3 - ig_{34} \hat{a}_4 - iJ \hat{a}_1 - \hat{f}_3^A - \hat{f}_3^B, \quad (\text{A7})$$

$$\partial_t \hat{a}_4 = -i\omega_4 \hat{a}_4 - ig_{34} \hat{a}_3 - iJ \hat{a}_2 - \hat{f}_4^A - (\hat{f}_4^B)^\dagger, \quad (\text{A8})$$

with

$$\begin{aligned} \hat{f}_j^A = & \frac{i}{\sqrt{2\pi}} \int_{-\infty}^{\infty} d\omega' \sqrt{\kappa(\omega')} \left[\hat{A}_j(\omega') \Big|_{t=t_0} e^{-i\omega'(t-t_0)} \right. \\ & \left. - i \sqrt{\frac{\kappa(\omega')}{2\pi}} \int_{t_0}^t dt' a_j(t') e^{-i\omega'(t-t')} \right], \end{aligned} \quad (\text{A9})$$

$$\begin{aligned} \hat{f}_j^B = & \frac{i}{\sqrt{2\pi}} \int_{-\infty}^{\infty} d\omega' \sqrt{\eta_j(\omega')} \left[\hat{B}_j(\omega') \Big|_{t=t_0} e^{-i\omega'(t-t_0)} \right. \\ & \left. - i \sqrt{\frac{\eta_j(\omega')}{2\pi}} \int_{t_0}^t dt' a_j(t') e^{-i\omega'(t-t')} \right]. \end{aligned} \quad (\text{A10})$$

We proceed by solving for the probe fields \hat{A}_k and the reservoir fields \hat{B}_k and substitute in Eqs. (A5)-(A8). Subsequently, we invoke the Markov approximation by ignoring the frequency dependence of the rates

$$\kappa(\omega') \approx \kappa, \quad \eta_k(\omega') \approx \eta_k. \quad (\text{A11})$$

This leads to a simpler set of equations

$$\partial_t \hat{a}_1 = -i\omega_1 \hat{a}_1 - ig \hat{a}_2 - iJ \hat{a}_3 + \hat{f}_1', \quad (\text{A12})$$

$$\partial_t \hat{a}_2 = -i\omega_2 \hat{a}_2 - ig \hat{a}_1 - iJ \hat{a}_4 + \hat{f}_2', \quad (\text{A13})$$

$$\partial_t \hat{a}_3 = -i\omega_3 \hat{a}_3 - ig \hat{a}_4 - iJ \hat{a}_1 + \hat{f}_3', \quad (\text{A14})$$

$$\partial_t \hat{a}_4 = -i\omega_4 \hat{a}_4 - ig \hat{a}_3 - iJ \hat{a}_2 + \hat{f}_4', \quad (\text{A15})$$

where

$$\hat{f}_1' = \sqrt{\kappa} \hat{A}_{1,\text{in}} - \frac{\kappa}{2} \hat{a}_1 + \sqrt{\eta_1} \hat{B}_{1,\text{in}} - \frac{\eta_1}{2} \hat{a}_1, \quad (\text{A16})$$

$$\hat{f}_2' = \sqrt{\kappa} \hat{A}_{2,\text{in}} - \frac{\kappa}{2} \hat{a}_2 - \sqrt{\eta_2} \hat{B}_{2,\text{in}} + \frac{\eta_2}{2} \hat{a}_2, \quad (\text{A17})$$

$$\hat{f}_3' = \sqrt{\kappa} \hat{A}_{3,\text{in}} - \frac{\kappa}{2} \hat{a}_3 + \sqrt{\eta_3} \hat{B}_{3,\text{in}} - \frac{\eta_3}{2} \hat{a}_3, \quad (\text{A18})$$

$$\hat{f}_4' = \sqrt{\kappa} \hat{A}_{4,\text{in}} - \frac{\kappa}{2} \hat{a}_4 - \sqrt{\eta_4} \hat{B}_{4,\text{in}} + \frac{\eta_4}{2} \hat{a}_4. \quad (\text{A19})$$

The Eqs. (A12)-(A15) together with Eqs. (A16)-(A19) constitute the Eq. (12) in the main text written in a compact form with the definition of the input fields given in Eq. (10) of the main text.

Appendix B: The Sain-Massey procedure for expanding inverses of singular matrices

Let an $n \times n$ meromorphic matrix function $A(z)$ have a Laurent expansion about z_0 :

$$A(z) = \sum_{j=0}^{\infty} (z - z_0)^j A_j, \quad (\text{B1})$$

where $A_j \in \mathbb{C}^{n \times n}$, $A_0 \neq 0$. Suppose the inverse $A^{-1}(z)$ exists in some (possibly punctured) disc centered at $z = z_0$. Then, $A^{-1}(z)$ can be expressed as a Laurent series:

$$A^{-1}(z) = \frac{1}{(z - z_0)^s} [X_0 + (z - z_0)X_1 + (z - z_0)^2 X_2 + \dots], \quad (\text{B2})$$

where s is a natural number called the order of the pole at $z = z_0$, and $X_0 \neq 0$.

To determine the value of s and compute the coefficient matrices X_k , we use the *Sain-Massey* method [39, 41, 42]. The method introduces an *augmented matrix*, defined as:

$$\mathcal{A}^{(t)} := \begin{pmatrix} A_0 & 0 & 0 & \dots & 0 \\ A_1 & A_0 & 0 & \dots & 0 \\ A_2 & A_1 & A_0 & \dots & 0 \\ \vdots & \vdots & \vdots & \dots & \vdots \\ A_t & A_{t-1} & A_{t-2} & \dots & A_0 \end{pmatrix}. \quad (\text{B3})$$

The pole order s is identified as the smallest value of t for which the rank condition

$$\text{rank } \mathcal{A}^{(t)} - \text{rank } \mathcal{A}^{(t-1)} = n \quad (\text{B4})$$

is satisfied, where n is the dimension of the matrix $A(z)$.

Once s is known, the coefficient matrices X_k are determined recursively for $k = 1, 2, \dots$ using

$$X_k = \sum_{j=0}^s \mathcal{G}_{0j}^{(s)} \left(\delta_{j+k,s} \mathbb{I} - \sum_{i=1}^k A_{i+j} X_{k-i} \right), \quad (\text{B5})$$

with the initial value X_0 given by the block $\mathcal{G}_{0s}^{(s)}$, here \mathbb{I} is the n -dimensional identity matrix.

Here, $\mathcal{G}_{0s}^{(s)}$ is part of the generalized inverse matrix $\mathcal{G}^{(s)}$, defined as:

$$\mathcal{G}^{(s)} := \begin{pmatrix} \mathcal{G}_{00}^{(s)} & \cdots & \mathcal{G}_{0s}^{(s)} \\ \vdots & \cdots & \vdots \\ \mathcal{G}_{s0}^{(s)} & \cdots & \mathcal{G}_{ss}^{(s)} \end{pmatrix}, \quad (\text{B6})$$

which represents the Moore–Penrose pseudo-inverse of the augmented matrix at $t = s$, i.e., $\mathcal{G}^{(s)} = (\mathcal{A}^{(s)})^+$ [43]. Here, the superscript (+) denotes the pseudoinverse of a matrix, which reduces to the standard inverse for a square, non-singular matrix. This approach systematically determines both the pole order and the expansion coefficients.

-
- [1] T. Kato, *Perturbation Theory for Linear Operators* (Springer, 1966).
- [2] Ş. K. Özdemir, S. Rotter, F. Nori and L. Yang, “Parity–time symmetry and exceptional points in photonics,” *Nat. Materials* **18**, 783 (2019).
- [3] R. El-Ganainy, K. G. Makris, M. Khajavikhan, Z. H. Musslimani, S. Rotter and D. N. Christodoulides, “Non-Hermitian physics and pt symmetry,” *Nat. Phys.* **14**, 11 (2018).
- [4] M. Parto, Y. G. N. Liu, B. Bahari, M. Khajavikhan and D. N. Christodoulides, “Non-Hermitian and topological photonics: optics at an exceptional point,” *Nanophotonics* **10**, 403 (2021).
- [5] W. D. Heiss, “The physics of exceptional points,” *J. Phys. A: Math. Theor.* **45**, 444016 (2012).
- [6] M. V. Berry and M. Wilkinson, “Diabolical points in the spectra of triangles,” *Proc. R. Soc. Lond. A. Math. Phys. Sc.* **392**, 15 (1984).
- [7] J. J. Peřina Jr., A. Miranowicz, G. Chimczak and A. Kowalewska-Kudłaszyk, “Quantum Liouvillian exceptional and diabolical points for bosonic fields with quadratic Hamiltonians: The Heisenberg-Langevin equation approach,” *Quantum* **6**, 883 (2022).
- [8] I. I. Arkhipov, A. Miranowicz, F. Minganti, Ş. K. Özdemir and F. Nori, “Dynamically crossing diabolic points while encircling exceptional curves: A programmable symmetric-asymmetric multimode switch,” *Nat. Comm.* **14**, 2076 (2023).
- [9] K. Thapliyal, J. P. Jr., G. Chimczak, A. Kowalewska-Kudłaszyk and A. Miranowicz, “Multiple quantum exceptional, diabolical, and hybrid points in multimode bosonic systems: I. Inherited and genuine singularities,” e-print arXiv:2405.01666 [quant-ph].
- [10] J. Peřina Jr., K. Thapliyal, G. Chimczak, A. Kowalewska-Kudłaszyk and A. Miranowicz, “Multiple quantum exceptional, diabolical, and hybrid points in multimode bosonic systems: II. Nonconventional \mathcal{PT} -symmetric dynamics and unidirectional coupling,” e-print arXiv:2405.01667 [quant-ph].
- [11] J. Wiersig, “Enhancing the sensitivity of frequency and energy splitting detection by using exceptional points: Application to microcavity sensors for single-particle detection,” *Phys. Rev. Lett.* **112**, 203901 (2014).
- [12] W. D. Heiss, “Exceptional points of non-Hermitian operators,” *J. Phys. A: Math. Gen.* **37**, 2455 (2004).
- [13] M. A. Miri and A. Alù, “Exceptional points in optics and photonics,” *Science* **363**, eaar7709 (2019).
- [14] F. Minganti, A. Miranowicz, R. W. Chhajlany and F. Nori, “Quantum exceptional points of non-Hermitian Hamiltonians and Liouvillians: The effects of quantum jumps,” *Phys. Rev. A* **100**, 062131 (2019).
- [15] J. Wiersig, “Review of exceptional point-based sensors,” *Photon. Res.* **8**, 1457 (2020).
- [16] W. Chen, Ş. K. Özdemir, G. Zhao, J. Wiersig and L. Yang, “Exceptional points enhance sensing in an optical microcavity,” *Nat.* **548**, 192 (2017).
- [17] H. Hodaei, A. U. Hassan, S. Wittek, H. Garcia-Gracia, R. El-Ganainy, D. N. Christodoulides and M. Khajavikhan, “Enhanced sensitivity at higher-order exceptional points,” *Nature* **548**, 187 (2017).
- [18] W. Langbein, “No exceptional precision of exceptional-point sensors,” *Phys. Rev. A* **98**, 023805 (2018).
- [19] H.-K. Lau and A. A. Clerk, “Fundamental limits and non-reciprocal approaches in non-Hermitian quantum sensing,” *Nat. Comm.* **9**, 1 (2018).
- [20] N. A. Mortensen, P. A. D. Gonçalves, M. Khajavikhan, D. N. Christodoulides, C. Tserkezis and C. Wolff, “Fluctuations and noise-limited sensing near the exceptional point of parity-time-symmetric resonator systems,” *Optica* **5**, 1342 (2018).
- [21] C. Wolff, C. Tserkezis and N. A. Mortensen, “On the time evolution at a fluctuating exceptional point,” *Nanophotonics* **8**, 1319 (2019).
- [22] M. Zhang, W. Sweeney, C. W. Hsu, L. Yang, A. D. Stone and L. Jiang, “Quantum noise theory of exceptional point amplifying sensors,” *Phys. Rev. Lett.* **123**, 180501 (2019).
- [23] C. Chen, L. Jin and R.-B. Liu, “Sensitivity of parameter estimation near the exceptional point of a non-Hermitian system,” *New J. Phys.* **21**, 083002 (2019).
- [24] J. Naikoo, R. W. Chhajlany and J. Kołodyński, “Multiparameter estimation perspective on non-Hermitian singularity-enhanced sensing,” *Phys. Rev. Lett.* **131**, 220801 (2023).
- [25] H. Loughlin and V. Sudhir, “Exceptional-point sensors offer no fundamental signal-to-noise ratio enhancement,” *Phys. Rev. Lett.* **132**, 243601 (2024).
- [26] J. Wiersig, “Prospects and fundamental limits in exceptional point-based sensing,” *Nat. Commun.* **11**, 2454 (2020).
- [27] K. Macieszczak, M. Guřa, I. Lesanovsky and J. P. Garrahan, “Dynamical phase transitions as a resource for quantum enhanced metrology,” *Phys. Rev. A* **93**, 022103 (2016).
- [28] S. Fernández-Lorenzo and D. Porrás, “Quantum sensing close to a dissipative phase transition: Symmetry breaking and criticality as metrological resources,” *Phys. Rev. A* **96**, 013817 (2017).

- (2017).
- [29] S. Wald, S. V. Moreira and F. L. Semião, “*In- and out-of-equilibrium quantum metrology with mean-field quantum criticality*,” *Phys. Rev. E* **101**, 052107 (2020).
 - [30] Y. Chu, S. Zhang, B. Yu and J. Cai, “*Dynamic framework for criticality-enhanced quantum sensing*,” *Phys. Rev. Lett.* **126**, 010502 (2021).
 - [31] W. Wu and C. Shi, “*Criticality-enhanced quantum sensor at finite temperature*,” *Phys. Rev. A* **104**, 022612 (2021).
 - [32] D. A. Steck, *Quantum and atom optics*, available online at <https://atomoptics.uoregon.edu/dsteck/teaching/>.
 - [33] J. Peřina, A. Miranowicz, J. K. Kalaga and W. Leoński, “*Unavoidability of nonclassicality loss in \mathcal{PT} -symmetric systems*,” *Phys. Rev. A* **108**, 033512 (2023).
 - [34] R. Wakefield, A. Laing and Y. N. Joglekar, “*Non-Hermiticity in quantum nonlinear optics through symplectic transformations*,” *Appl. Phys. Lett.* **124**, 201103 (2024).
 - [35] C. Weedbrook, S. Pirandola, R. Garcia-Patrón, N. J. Cerf, T. C. Ralph, J. H. Shapiro and S. Lloyd, “*Gaussian quantum information*,” *Rev. Mod. Phys.* **84**, 621 (2012).
 - [36] A. Ferraro, S. Olivares and M. G. A. Paris, *Gaussian states in continuous variable quantum information* (Bibliopolis, Napoli, 2005).
 - [37] S. L. Braunstein and C. M. Caves, “*Statistical distance and the geometry of quantum states*,” *Phys. Rev. Lett.* **72**, 3439 (1994).
 - [38] S. M. Kay, *Fundamentals of statistical signal processing: estimation theory* (Prentice-Hall, Hoboken, 1993).
 - [39] M. Sain and J. Massey, “*Invertibility of linear time-invariant dynamical systems*,” *IEEE Trans. Autom. Control* **14**, 141 (1969).
 - [40] F. Zhou, “*A rank criterion for the order of a pole of a matrix function*,” *Lin. Alg. App.* **362**, 287 (2003).
 - [41] P. G. Howlett, “*Input retrieval in finite dimensional linear systems*,” *J. Australian Math. Soc. Ser. B. App. Math.* **23**, 357 (1982).
 - [42] P. Howlett and K. Avrachenkov, “*Laurent Series for the Inversion of Perturbed Linear Operators on Hilbert Space*,” in *Optimization and Related Topics*, ed. A. Rubinov and B. Glover (Springer US, Boston, MA, 2001) pp. 325–342.
 - [43] K. E. Avrachenkov, J. A. Filar and P. G. Howlett, *Analytic perturbation theory and its applications* (SIAM, 2013).